Thin Solid Films 591 (2015) 316–322

Contents lists available at ScienceDirect

Thin Solid Films

journal homepage: www.elsevier.com/locate/tsf

Niobium–niobium oxide multilayered coatings for corrosion protection of proton-irradiated liquid water targets for [^{18}F] production

Hanna Skliarova [a,b,*], Marco Renzelli [c], Oscar Azzolini [a], Daniele de Felicis [c], Edoardo Bemporad [c], Richard R. Johnson [d], Vincenzo Palmieri [a,e]

[a] National Institute of Nuclear Physics, Legnaro National Laboratories, Viale dell'Università, 2, 35020 Legnaro, Padua, Italy
[b] University of Ferrara, Ferrara, Italy
[c] University of Rome "Roma TRE", Via della Vasca Navale, 79, 00146 Rome, Italy
[d] BEST Cyclotron Systems Inc., 8765 Ash Street Unit 7, Vancouver BC V6P 6T3, Canada
[e] University of Padua, Padua, Italy

ARTICLE INFO

Available online 10 March 2015

Keywords:
Sputtering
Niobium
Niobium oxide
Multilayers
X-ray diffraction
Diffusion barrier
Scanning electron microscopy
Focus ion beam

ABSTRACT

Chemically inert coatings on Havar® entrance foils of the targets for [^{18}F] production via proton irradiation of enriched water at pressurized conditions are needed to decrease the amount of ionic contaminants released from Havar®. During current investigation, magnetron sputtered niobium and niobium oxide were chosen as the candidates for protective coatings because of their superior chemical resistance. Aluminated quartz substrates allowed us to verify the protection efficiency of the desirable coatings as diffusion barriers. Two modeling corrosion tests based on the extreme susceptibility of aluminum to liquid gallium and acid corrosion were applied. As far as niobium coatings obtained by magnetron sputtering are columnar, the grain boundaries provide a fast diffusion path for active species of corrosive media to penetrate and to corrode the substrate. Amorphous niobium oxide films obtained by reactive magnetron sputtering showed superior barrier properties according to the corrosion tests performed. In order to prevent degrading of brittle niobium oxide at high pressures, multilayers combining high ductility of niobium with superior diffusion barrier efficiency of niobium oxide were proposed. The intercalation of niobium oxide interlayers was proved to interrupt the columnar grain growth of niobium during sputtering, resulting in improved diffusion barrier efficiency of obtained multilayers. The thin layer multilayer coating architecture with 70 nm bi-layer thickness was found preferential because of higher thermal stability.

1. Introduction

Radioisotopes find applications all around the world, making a great contribution to the improvement of health care. [^{18}F] ($t_{1/2}$ = 109.7 h, 97% β^+) is the most widely used (>95%) radioisotope in Positron Emission Tomography, involved essentially in all scans for oncology and most scans in neurology. [^{18}F] is produced almost exclusively through irradiation of enriched water targets by cyclotron accelerated proton beam. The cyclotron target for [^{18}F] production is a small volume of [^{18}O]-enriched water sealed between target chamber and entrance foil for the proton beam [1]. The irradiation induced water radiolysis results in production of highly reactive species (such as radicals, ions, and H_2O_2), making water an extremely corrosive media. The use of suitable material for target chamber and entrance foil is mandatory. This appropriate material has to fulfill a number of mechanical and thermal requirements and also must have high corrosion resistance to irradiated water [2,3]. Thus chemically inert bulk niobium is used for target chamber. Havar® foils are usually used for high pressure target application because of their high strength and flexibility [4], allowing the use of thin beam windows for minimal beam attenuation.

Designing the target for radioisotope production, it is not always possible to find the material that corresponds all the requirements at the same time. The use of thermally and mechanically suitable substrate materials, protected by chemically resistant coating, can be a compromise. It was shown that the use of sputtered niobium coating on Havar® entrance foils decreases more than ten times [2] the amount of ionic long-lived impurities during [^{18}F] production, nevertheless the amount is still significant.

The main corrosion damage of cyclotron target entrance foils is caused by the appearance of high local concentrations of reactive species on the foil surface. The species diffuse fast through the

* Corresponding author at: National Institute of Nuclear Physics, Legnaro National Laboratories,Viale dell'Università, 2, 35020 Legnaro, Padua, Italy. Tel.: +39 3201837213.
E-mail addresses: Hanna.Skliarova@lnl.infn.it (H. Skliarova), marco.renzelli@uniroma3.it (M. Renzelli), Oscar.Azzolini@lnl.infn.it (O. Azzolini), daniele.defelicis@uniroma3.it (D. de Felicis), edoardo.bemporad@uniroma3.it (E. Bemporad), richard.johnson@teambest.com (R.R. Johnson), Vincenzo.Palmieri@lnl.infn.it (V. Palmieri).

http://dx.doi.org/10.1016/j.tsf.2015.03.011

protective film towards Havar® substrate and interact chemically with the substrate. The grain boundaries through the film offer the main diffusion paths for such reactive species. The amorphous coatings are characterized by the structure irregularity and the absence of typical structural defects of the crystalline state, such as dislocations and grain boundaries, and thus provide higher diffusion barrier efficiency [5–7].

Metal oxides are known to form an amorphous structure easier than metals. The current investigation was focused on the comparison of crystalline niobium sputtered coatings and amorphous niobium oxide coatings obtained by reactive sputtering deposition. Oxide coatings are known to be brittle [8] and this property can hinder the use of pure niobium oxide coating on Havar® entrance beam foil under pressurized conditions. The multilayer structure is known to be a way to improve toughness of ceramics thin films inserting layers with higher plasticity (metallic) [9]. The toughness enhancement is realized through the following three main mechanisms: crack deflection at interface between layers, ductile interlayer ligament bridging and crack tip blunting due to nanoplasticity at the interface. It was realized for the number of metal–ceramic multilayer systems [10–12]. Thereby Nb/Nb_2O_5 multilayer coatings were put forward with the aim to avoid the problem of the oxide brittleness.

The objective of the work was to determine the influence of the microstructure, in particular the impact of amorphization, of deposited niobium, niobium oxide and Nb/Nb_2O_5 multilayers on the barrier properties of the coatings in order to find the best protective coating for cyclotron target entrance foils. The use of an improved protective coating will significantly decrease the amount of ionic impurities from Havar® during [^{18}F] production and thus increase the specific activity of the final radiopharmaceutical [^{18}F].

2. Experimental details

2.1. Sputtering

The coatings were deposited by DC sputtering with a 2 in. diameter planar magnetron source in a cylindrical 316L stainless steel vacuum chamber of 11 cm diameter and 26 cm in length. The substrates were placed onto a planar substrate holder at 6 cm from the cathode. Before sputtering, the chamber was initially pumped to a base pressure of $3°10^{-4}$ Pa by a Pfeiffer turbo molecular pump of 360 l/min and a primary pump Varian Tri Scroll Pump of 12 m^3/h.

The niobium sputtering targets were machined from a high grade bulk Nb (99.99% purity). The niobium thin film deposition was performed with argon (99.9999% purity) as sputtering gas. The niobium oxide films were obtained by reactive magnetron sputtering in the same sputtering system using a mixture of argon and oxygen (99.9999% purity) gases.

1.6 μm Nb coatings were deposited at 0.3 Pa using 3 sccm argon flux and 0.5 A DC without heating or cooling down the substrate (~230 °C) during 30 min (see Table 1). The pressure for Nb deposition was chosen according to the results obtained in previous investigations [13].

The investigation of optimal parameters for sputtering of niobium oxide for sufficient deposition rate of stoichiometric niobium oxide by reactive sputtering was described in previous work [13]. Reactive sputtering of stoichiometric niobium oxide was performed at 1 Pa total sputtering gas pressure using 3 sccm of Ar and 7 sccm of O_2 and 0.5 A DC. The value of deposition rate for the niobium oxide by reactive sputtering of 0.2 nm/s was used for the estimation of the thickness of niobium oxide layer in multilayers (see Table 1).

The multilayer architecture was shown to influence the mechanical stability of multilayer [14–16]. Thus, multilayer samples with different periodicity, were prepared by fixing the argon flux at 3 sccm, and periodically switching the oxygen flux from 0 sccm to 7 sccm. The deposition parameters used are resumed in Table 1. We have investigated two different architectures, preparing coatings made by 30 thin layers (Thin ML) and by 6 thick layers (Thick ML). In both cases, the Nb_2O_5 thickness was always intended to be ten times thinner than Nb (see Table 1). In order to perform reliable multilayer depositions, the oxygen flux was controlled with appropriate automated feedback. The coating with thick layers was prepared also by thermal oxidation of Nb layer introducing the maximum oxygen flux, immediately after each layer deposition (Oxidized ML).

Table 1
Deposition parameters for multilayer coatings.

Sample number	Nb	Nb_2O_5	Thin ML	Thick ML	Oxidized ML
Method	Sputtering	Reactive sputtering	Fine layers	Thick layers	Thermal oxidation
Ar flux, sccm	3	3	3	3	3
O_2 flux, sccm	0	7	0/7	0/7	0/100
Work pressure, Pa	0.3	1.2	0.3/1	0.3/1	0.3/22.05
Number of bi-layers	–	–	30	6	6
Expected Nb layer thickness, nm	–	–	30	220	220
Expected Nb_2O_5 layer thickness, nm	–	–	3	25	–
Measured bi-layer thickness, nm	–	–	70	320	220–280
Thickness, μm	1.6	1.6	2.5	2.5	1.9

2.2. Diffusion barrier efficiency tests

Since the direct test of a protective coating on Havar® entrance foil on a cyclotron facility is not a routine operation, the preliminary tests of the coatings anticorrosion efficiency were required. Since the corrosion of coated cyclotron target entrance foils can be described principally by the diffusion of the reactive species, produced by water radiolysis through a chemically inert film towards the Havar® substrate, the control of the diffusion barrier efficiency can be used for the protective coatings evaluation.

In literature, the most described technique for the diffusion barrier efficiency evaluation [17–19] was based on observation of copper atoms penetration through the grain boundaries of metallic coatings at high temperatures. We performed two faster and simpler methods for evaluation of the film diffusion barrier efficiency: we used an Al underlayer behind niobium-based coating to reveal pore and weak grain boundary sites by visible products of corrosion. Quartz samples 9 × 9 × 1 mm (optical finishing) covered with 2.5 μm of aluminum (by DC magnetron sputtering) were used as substrates, in order to minimize the effect of substrate roughness on the protective coating quality. The first test was performed by immersing the coated samples into 10% HCl solution for 10 min at 30 °C. Aluminum is reactive, and Nb and Nb_2O_5 are inert to this solution. Acid penetrates through pores/voids/weak grain boundaries in the Nb-based film and reacts with the Al underlayer, producing H_2 bubbles (see Fig. 1). We evaluated the results in a scale from 1 to 5, where, respectively: 1 means minimal amount of

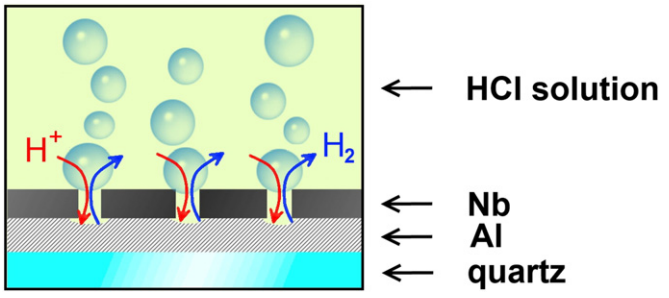

Fig. 1. Schematic explanation of diffusion barrier efficiency test of inert Nb coating in acid solution.

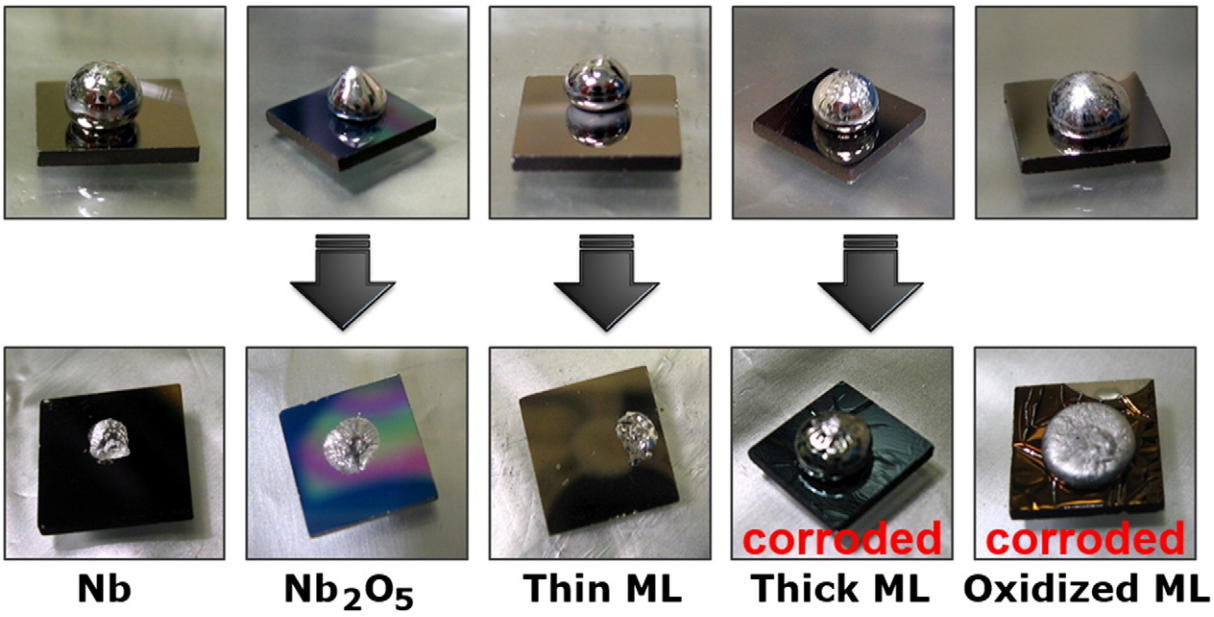

Fig. 2. The liquid gallium test for investigated coatings.

H_2 bubbles and high diffusion barrier efficiency, and 5 means lowest efficiency.

The liquid gallium test was carried out by heating the aluminated quartz samples coated with the investigated Nb-based coatings (the same preparation of samples done in previous test) with liquid Ga droplets during 30 h at 200 °C. Nb and Nb_2O_5 are inert for liquid Ga, while aluminum is well-known to be corroded fast by liquid Ga causing the so called liquid-metal embrittlement. The mechanism can be described by the rapid liquid Ga penetration along the Al grain boundaries [20–22] that results in a substantial loss of cohesion [23]. When prolonged defects, such as pores/voids/weak grain boundaries were present, liquid Ga penetrated through the film, the Al under-layer became liquid and the protective film was ruined. That was what we had visually detected. The diffusion barrier efficiency tests were described more in details in our previous work [13].

2.3. Direct porosity control

The topographies of every sample were acquired using Leica DCM3D non-contact optical profilometer in confocal mode, searching for droplet-like defects and trough-thickness holes. The raw data from the instrument were used as an input for the software Sensofar LeicaMap, computing the total area not covered by the film due to the holes.

The surface imaging of the sample was done using a FEI (Philips) XL30 LaB_6 scanning electron microscope (SEM) using both secondary electron (SE) and backscattered electron (BSE) imaging. The SE imaging resulted more fruitful at high magnifications, highlighting the holes as black areas (no secondary electron production) and the macroparticles as bright areas (droplets are prone to charging due to the bad electrical contact between droplets and surrounding material, thus producing many secondary electrons) meanwhile BSE imaging was used especially at low magnifications giving the better contrast.

2.4. Microstructure analysis

All samples were cross sectioned using Focused Ion Beam (FIB) technology to assess the grain dimension and the film microstructure control. The standard FIB cross sectioning procedure with the FEI Helios NanoLab 600 equipped with a FEG electron column and a Ga^+ ion was performed using a ion current of 9.3 nA for milling and 0.92 nA for cleaning, then imaging with electron (for maximum resolution, using immersion lens trough lens detector) and ion probe (for maximum crystallographic contrast, using continuous dynode electron multiplier detector). At low resolution and large field of view it was used, with both probes an Everhart–Thornley Detector, without immersion lens.

The investigated coatings were sputtered also onto $9 \times 9 \times 1$ mm quartz samples for X-ray diffraction investigation (XRD), in the same deposition runs, together with the aluminated quartz samples for diffusion barrier efficiency tests. The XRD investigation was carried out by performing the θ–θ Goniometer scan in Bragg–Brentano configuration with 2θ from 10° to 100° (180°–2θ is the angle between the X-ray source, the substrate and the detector). The 1.54 Å Cu-Kα X-ray was used to observe X-ray diffraction of thin films with a PANalytical (ex-Philips) PW3040/60 Diffractometer. The data of the diffracted beam intensity dependence on 2θ were plotted and fitted by the X'Pert

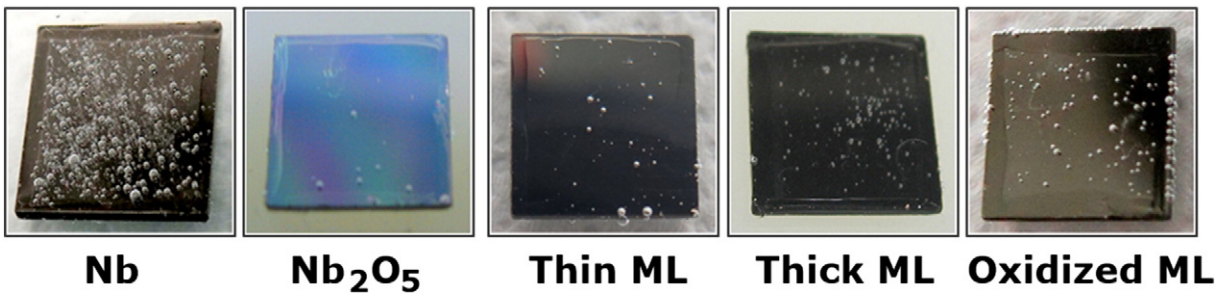

Fig. 3. The acid test for the investigated coatings.

Highscore software in order to obtain the peak position and the integral breadth.

The shape of the graphs was used to provide a general recognition of crystalline or amorphous structure. The average grain size was determined using Debye–Scherrer formula:

$$D = \frac{0.9 \cdot \lambda}{B \cdot \cos\theta} \quad (1)$$

being λ the wave length of the X-ray source, in case of Cu-Kα X-ray λ = 1.54056 Å and B the Bragg XRD peak breadth.

Atomic force microscopy (AFM) analysis was performed using a NT-MDT Smena AFM, operated in non-contact mode, equipped with the NOVA software. The same Sensofar LeicaMap software used with the profilometer was used with the AFM output files, using same roughness evaluation standards in both measurements.

3. Results

3.1. Niobium coating

The niobium coating resisted to liquid gallium droplet exposition for more than 30 h. The niobium coating showed incomplete wettability by liquid gallium droplet with the contact angle <90°, and after the removal of the liquid Ga droplet some traces of it remained on the top of the surface (Fig. 2). Niobium coating performed low efficiency as diffusion barrier in the test with the acid solution (see Fig. 3).

Fig. 4 represents the FIB SEM analysis of the cross-section of the niobium coating using electron beam [Fig. 4(a)]. Since the contrast on the image obtained with electron gun is not enough, for grain size estimation the ion beam imaging was used [Fig. 4(b)]. Fig. 4(c) represents the image of the surface of the film obtained by high resolution SEM. From Fig. 4(a, b) a dense microstructure with columns through the coating can be distinguished, with the average grain size of 180 nm.

The XRD (see Fig. 5) of pure niobium film represents the crystalline microstructure with the preferred 110 orientation and the average crystallite size calculated by the Debye–Scherrer formula of about 17 nm.

3.2. Niobium oxide coating

Stoichiometric niobium oxide films were transparent and had an amorphous structure according to the XRD (see Fig. 5). The Nb_2O_5 coatings showed superior protection efficiency both against the liquid gallium corrosion and the acid corrosion than the niobium thin films (Figs. 2, 3). Niobium oxide coatings, as niobium coatings, showed incomplete wettability by liquid Ga, resisted to liquid gallium penetration for more than 30 h, and retained some traces after removal of the liquid Ga droplet (Fig. 2).

Fig. 6 shows the surface morphology obtained by high resolution SEM and the cross-section of the thin film obtained by the FIB SEM. The direct observation of the microstructure confirmed the glass-like amorphous structure analyzed by the XRD. The film was dense and no grain boundaries were observed in the film cross-section.

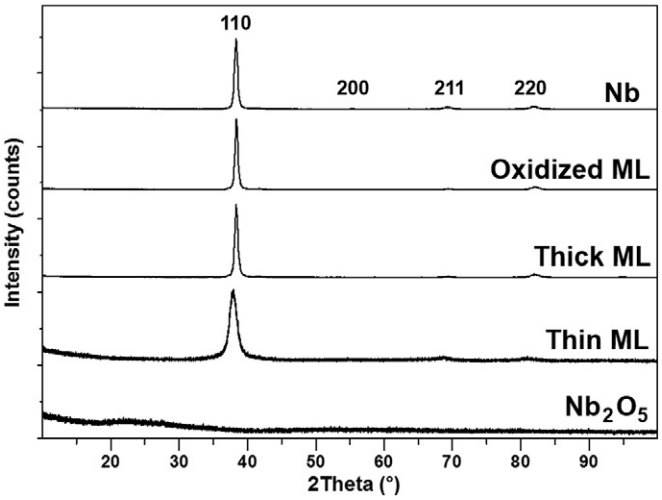

Fig. 5. XRD of investigated coatings.

Fig. 7 represents the AFM analysis of 3 μm × 3 μm surface of the niobium [Fig. 7(a)] and the niobium oxide [Fig. 7(b)] coatings. The surface morphologies of both coatings correspond to the ones obtained by SEM (crystalline niobium and glass-like amorphous niobium oxide). The average surface roughness (R_a parameter) measured by the AFM was respectively 9.2 ± 2.5 nm for niobium coating and 5.5 ± 1.1 nm for niobium oxide coating.

3.3. Multilayers

The SEM picture in Fig. 8(a) displays the multilayer section of the 30 thin layers of the Thin ML coating. It allows estimating an average bi-layer (layer of Nb + layer of Nb_2O_5) thickness of about 70 nm. From Fig. 8(b) the thickness of the Nb and the Nb_2O_5 layers in the Thick ML coating was estimated about 260 nm and 160 nm correspondingly. Fig. 8(c) shows the clear multilayer structure of the Oxidized ML coating with the layer thickness of about 220–280 nm. The average grain sizes for Thick ML and Oxidized ML are represented in Table 2.

The XRD patterns of the multilayer coatings are presented in Fig. 5. The XRD patterns of multilayer coatings with thick Nb layer architecture (Thick ML and Oxidized ML) were found quite similar to the one of pure Nb coating. Otherwise the thin layer multilayer pattern (Thin ML) showed significant peak broadening proving the crystallite size decrease. The cubic lattice parameters and the average crystallite sizes for the investigated coatings obtained from the XRD data are presented in Table 2.

The decrease of each bi-layer thickness resulted in a significant decreasing of the average crystallite size of niobium (see Table 2), passing

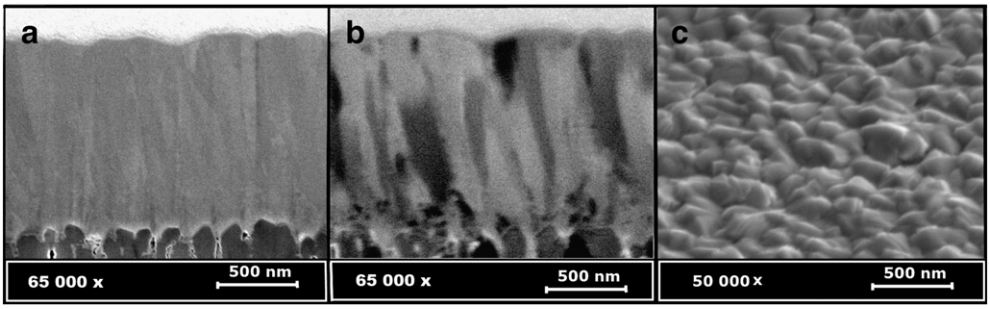

Fig. 4. High resolution SEM of Nb coating: a) FIB SEM of cross-section using electron beam; b) FIB SEM of cross-section using ion beam; c) SEM of the film surface.

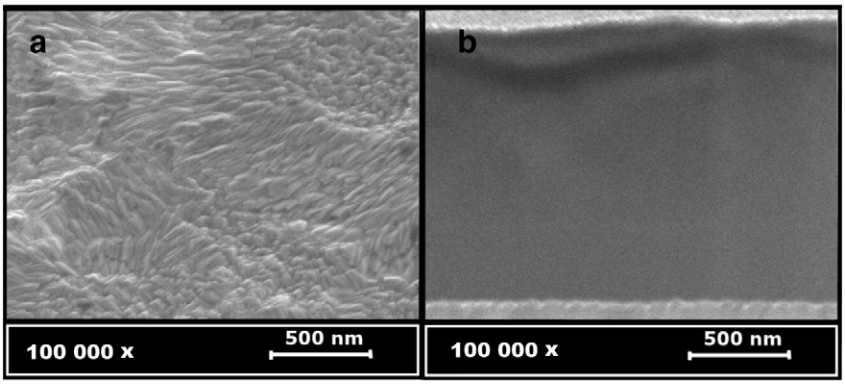

Fig. 6. SEM of amorphous niobium oxide: a) top view; b) FIB-SEM of cross-section.

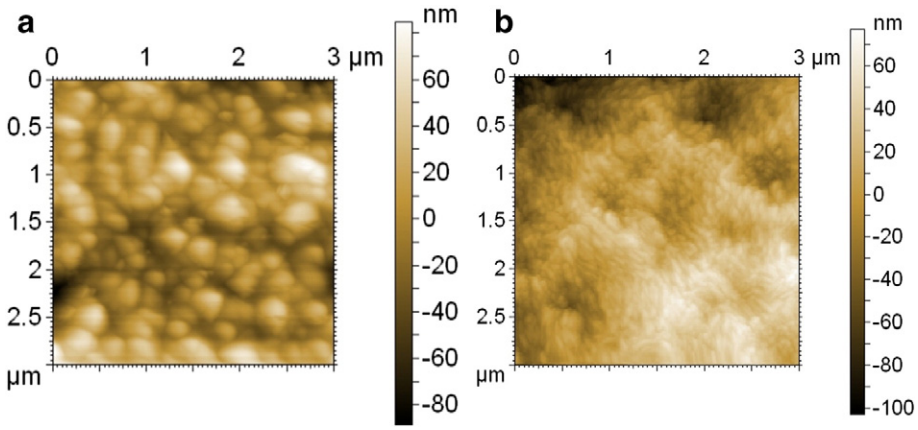

Fig. 7. AFM analysis of surface roughness of a) niobium; b) niobium oxide.

from 16 nm for the sample Thick ML and 18 nm for the Oxidized ML to a 5 nm for the Thin ML sample.

The multilayer Nb–Nb_2O_5 coatings showed an incomplete wettability by liquid gallium (Fig. 2). Also the resistance to the acid solution (see Fig. 3) was similar to that of niobium oxide and higher compared to the simple Nb coating.

While the thin-layered multilayer coating (Thin ML) showed good resistance to liquid Ga penetration, the thick-layered multilayer coatings (Thick ML, Oxidized ML) did not resist (see Fig. 2).

The optical profilometry of the area of 200 µm × 200 µm of each coating was used to estimate the total area not covered by the film, due to the holes deeper than 0.5 µm. The data of optical profilometry are presented in Table 2. The profilometry data proved that the bad performance of pure Niobium coatings in the acid test was attributed not just to the weak grain boundaries through the film but also to the pinholes generated during or after the deposition, when the weak-bonded macroparticles were removed.

4. Discussion

According to the SEM images of the cross section, the Nb coating had a columnar microstructure, as it was expected, with a thickness of 1.6 µm. The same thickness was estimated for the niobium oxide monolayer coating. No additional energy input (no heating, no ion pinning due to the biasing of the sample) during the deposition of niobium oxide resulted in an amorphous structure, which is beneficial for the diffusion barrier purposes. The Thin ML, the fine layered multilayer, was found to be 2.5 µm thick, instead of the expected 1 µm. This sample showed the biggest deviation from the expected thickness, because the oxide layers appeared to be almost as thick as the metallic ones, instead

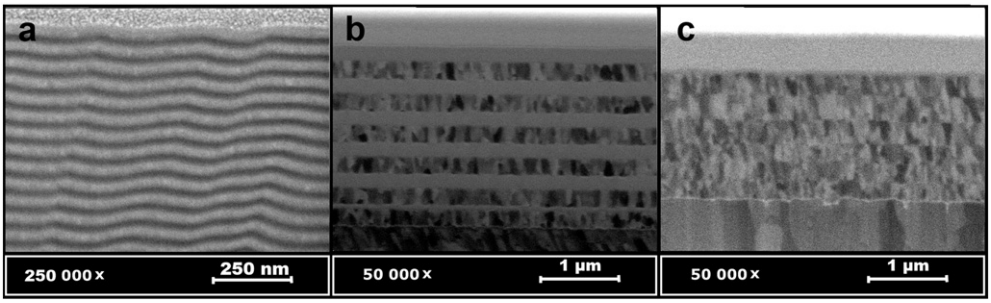

Fig. 8. FIB-SEM of the cross-sections of sputtered Nb–Nb_2O_5 multilayers: a) Thin ML; b) Thick ML; c) Oxidized ML.

Table 2
Microstructure and barrier properties.

Sample number	Nb	Nb_2O_5	Thin ML	Thick ML	Oxidized ML
Method	Sputtering	Reactive sputtering	Fine layers	Thick layers	Thermal oxidation
Average crystallite size (XRD), nm	17	Amorphous	5	16	18
Average grain size (SEM), nm	180	Amorphous	–	70	80
Cubic lattice parameter, Å	3.321	–	3.362	3.317	3.318
Area covered by holes deeper 0.5 μm (optical profilometry), %	1	0.01	0	0	0
Liquid Ga corrosion	Resisted	Resisted	Resisted	Corroded	Corroded
Acid test (1 ÷ 5)	5	1	1	2	2

of being ten times thinner, as it was planned. This could be explained due to the big inertia of the pumping system when modulating the open-close duty cycle of the oxygen flux and thus broader interface between niobium and niobium oxide. Moreover, the deposition rate of niobium oxide by the reactive sputtering in the case of multilayer was higher, because the Nb target was "cleaned" by argon plasma during each niobium layer deposition.

The grain size of niobium depends on the thickness of the film: increasing the film thickness the grains are wider, due to the V-shape of the columns themselves; so to achieve small crystal sizes it is necessary to stop the column growth. The niobium layers intercalated with the niobium oxide layers were shown to decrease the grain size of niobium coatings, because amorphous oxide stopped the columns growth, while metallic niobium nucleated again in the layer after.

The Thick ML is a multilayer of amorphous oxide and crystalline metallic layers. As explained before, the use of an amorphous oxide layer stopped the growth of the grain columns in metallic niobium. As expected, there was no microstructural coherence between the observed layers. For this reason the sample was considered a good diffusion barrier candidate. Also, in this case the sample was thicker than expected; however the difference with the expected thickness was lower than the fine multilayer one, giving credence to the hypothesis that the reason was the pumping system inertia. The SEM image of Oxidized ML observed using ions [Fig. 8(c)] clearly showed that the oxidation step between layers deposition was useful to stop column growth and restart it layer-by-layer, resulting in the average grain size of about 80 nm. The last sample Oxidized ML proved that the very thin oxidized layer formed between layers was enough to stop the grain growth without using "true" layers of Nb_2O_5. The sample was a bit thicker than expected, due to the oxygen addition during deposition stops. For the Thin ML system we had not observed the grains of the Nb layer with FIB.

The average crystallite size of the Nb layers in the Thick ML and Oxidized ML according to the XRD data (see Table 2) was found similar to the pure niobium coating. This means that the crystallite size had not the same linear dependence related to the layer thickness as happened with the grain size. Also, the cubic lattice parameter for Thick ML and Oxidized ML multilayer coatings did not deviate a lot from pure niobium coating. The cubic lattice parameter calculated for the Nb layers in Thick ML and Oxidized ML was closer to the value of the tabulated bulk Nb (3.300 Å) than the one estimated for pure niobium coating. This can be attributed to the decrease of the intrinsic stress in the Nb layers due to a smaller thickness of the single layer. Otherwise the XRD analysis of Thin ML gave the average crystallite size and cubic lattice parameter rather different from pure niobium coating (see Table 2). This can be referred both to the significant crystallite size decrease (~5 nm) and to oxygen atom incorporation into the Nb lattice.

The pure niobium coatings showed a low performance in the diffusion barrier test with the acid solution, attributed both to the grain boundaries across the film thickness and to a high density of other defects, like pinholes and macroparticles, originated during the thin film deposition. The last ones were monitored with the optical profilometer and with low resolution SEM. The resistance of Niobium coating to the liquid gallium penetration could be explained by the incomplete wettability due to the surface "lotus effect" that came out from the high roughness of the niobium coating. The stoichiometric niobium oxide coatings showed a superior efficiency as diffusion barrier both for acid and liquid gallium, thanks to the amorphous structure without grain boundaries.

The presence of the amorphous niobium oxide interlayers in all multilayer coatings had provided them higher efficiency than pure niobium coatings in the acid test. However, the multilayer coatings with 6 thick layers Thick ML and Oxidized ML had degraded and were corroded during the liquid Ga test. We suppose that, so far, as niobium and niobium oxide had different thermal expansion coefficients, some microcracks could appear during heating to 200 °C, and could allow the penetration of liquid gallium. For the Oxidized ML we observed a bubble-like feature on the surface (Fig. 9), probably due to the oxidation steps, capable of carrying the Ga trough the coating to the underlying Al. The "lotus effect" does not influence the liquid gallium test for multilayer coatings because the upper niobium oxide layer had lower roughness. The Thin ML coating showed the high diffusion barrier efficiency comparable to the one of Nb_2O_5 and resisted also to heating/cooling cycles in the liquid Ga test. It can be attributed to the presence of a higher number of interfaces, which prevent the movement of the dislocations. These result in plastic deformation in the materials and stop (interrupt) the propagation of the micro-cracks responsible for the fractures in the Nb_2O_5 layer. In addition to this, the fine layered structure of Thin ML allows better thermal expansion coefficient mismatch accommodation than in the case of the Thick ML sample. Therefore, the Thin ML coating was considered to be the most promising candidate for the protective coating of the cyclotron target beam window operating at pressurized conditions.

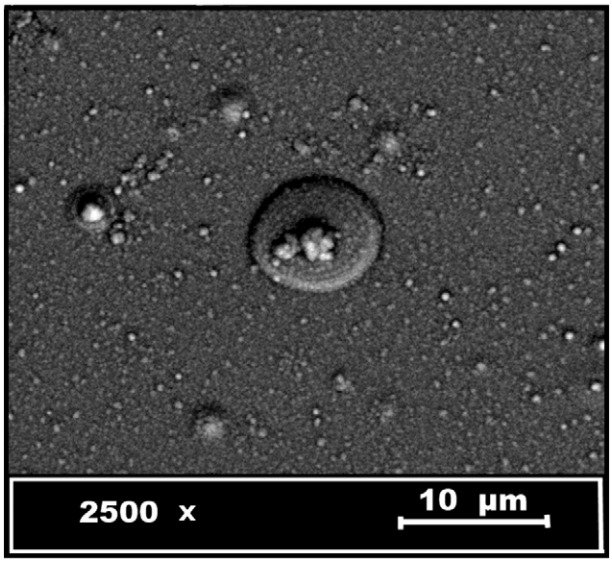

Fig. 9. SEM of the defects on the M 3 multilayer surface.

5. Conclusions

The use of an appropriate multilayer architecture was found sufficient to combine the properties of the niobium and the niobium oxide layers with the aim to reach a high diffusion barrier efficiency and high thermal stability. The intercalation of the Nb_2O_5 interlayers was proved to interrupt the columnar grain growth of Nb during sputtering, resulting in an improved diffusion barrier efficiency. For the thick layer multilayers the grain size of Nb in the crystalline metallic layer was found to increase with the layer thickness, however the crystallite size was similar to the one of the pure niobium coating. The decrease of the bi-layer thickness from 280 nm to 70 nm resulted in the decrease of the grain size and the average crystallite size of Nb layer. The thin layer multilayer coating architecture with 70 nm bi-layer thickness was found preferential because of higher thermal stability.

Acknowledgments

This work was financed by the V Group of INFN for Accelerator and Interdisciplinary Physics, with a contribution from BEST Cyclotrons.

We are thankful to Prof. G. Fiorentini, Dr. G. Cuttone, Prof. M. Carpinelli, and Dr. M. Bonardi for their precious support and all the staff of the INFN-LNL Service for Material Science and Technology applied to Nuclear Physics for their constant help.

References

[1] M. Guillaume, A. Luxen, B. Nebeling, M. Argentini, J.C. Clark, V.W. Pike, Recommendations for fluorine-18 production, Appl. Radiat. Isot. 42 (1991) 749.
[2] J.S. Wilson, M.A. Avila-Rodriguez, R.R. Johnson, A. Zyuzin, S.A. McQuarrie, Niobium sputtered Havar foils for the high-power production of reactive [^{18}F]fluoride by proton irradiation of [^{18}O]H_2O targets, Appl. Radiat. Isot. 66 (2008) 565.
[3] A.D. Roberts, L.C. Daniel, R.J. Nickles, A high power target for the production of [^{18}F] fluoride, Nucl. Instrum. Methods Phys. Res. Sect. B 99 (1995) 797.
[4] Cyclotron produced radionuclides: operation and maintenance of gas and liquid targets, IAEA Radioisotopes and Radiopharmaceuticals Series, International Atomic Energy Agency, Vienna, 2012.
[5] M.-A. Nicolet, Diffusion barriers in thin films, Thin Solid Films, Elsevier Sequoia S.A., Lausanne, 1978. 415.
[6] I.V. Zolotuhin, Y.E. Kalinin, Amorphous metallic materials, Prog. Phys. Sci. 160 (1990) 75.
[7] M. Mehmood, E. Akiyama, H. Habazaki, A. Kawashima, K. Asami, K. Hashimoto, Effects of nanocrystalline heterogeneity on the corrosion behavior of sputter-deposited chromium–niobium alloys, Corros. Sci. 42 (2000) 361.
[8] J.C. Grosskreutz, Mechanical properties of metal oxide films, J. Electrochem. Soc. 116 (1969) 1232.
[9] Z. Chen, J.J. Mecholsky, Control of strength and toughness of ceramic/metal laminates using interface design, J. Mater. Res. 8 (1993) 2362.
[10] G.S. Was, J.W. Jones, C.E. Kalnas, L.J. Parfitt, M. Goldiner, Role of ion beam assisted deposition in the synthesis and fracture of metal–ceramic multilayers, Surf. Coat. Technol. 65 (1994) 77.
[11] Q. Yang, D.Y. Seo, L.R. Zhao, Multilayered coatings with alternate pure Ti and TiN/CrN superlattice, Surf. Coat. Technol. 177–178 (2004) 204.
[12] C.J. Tavares, L. Rebouta, E. Alves, A. Cavaleiro, P. Goudeau, J.P. Rivière, A. Declemy, A structural and mechanical analysis on PVD-grown (Ti, Al)N/Mo multilayers, Thin Solid Films 377–378 (2000) 425.
[13] H. Skliarova, O. Azzolini, O. Cherenkova-Dousset, R.R. Johnson, V. Palmieri, Niobium-based sputtered thin films for corrosion protection of proton-irradiated liquid water targets for [^{18}F] production, J. Phys. D. Appl. Phys. 47 (2014) 045306.
[14] D.M. Marulanda, J.J. Olaya, U. Piratoba, A. Mariño, E. Camps, The effect of bilayer period and degree of unbalancing on magnetron sputtered Cr/CrN nano-multilayer wear and corrosion, Thin Solid Films 519 (2011) 1886.
[15] L. Major, J.M. Lackner, M. Kot, M. Janusz, B. Major, Contribution of TiN/Ti/a-C:H multilayers architecture to biological and mechanical properties, Bull. Pol. Acad. Sci. Tech. Sci. 62 (2014) 565.
[16] E. Bemporad, M. Sebastiani, F. Casadei, F. Carassiti, Modelling, production and characterisation of duplex coatings (HVOF and PVD) on Ti–6Al–4V substrate for specific mechanical applications, Surf. Coat. Technol. 201 (2007) 7652.
[17] C. Li, J.H. Hsieh, Z.Z. Tang, Study on the amorphous Ta–Zr films as diffusion barrier in Cu metallization, J. Vac. Sci. Technol. A 26 (2008) 980.
[18] S. Young-Hoon, S. Yukihiro, Diffusion barrier property of TiN and TiN/Al/TiN films deposited with FMCVD for Cu interconnection in ULSI, Sci. Technol. Adv. Mater. 5 (2004) 399.
[19] S.-Y. Jang, S.-M. Lee, H.-K. Baik, Tantalum and niobium as a diffusion barrier between copper and silicon, J. Mater. Sci. Mater. Electron. 7 (1996) 271.
[20] R.C. Hugo, R.G. Hoagland, The kinetics of gallium penetration into aluminum grain boundaries—in situ TEM observations and atomistic models, Acta Mater. 48 (2000) 1949.
[21] E. Pereiro-López, W. Ludwig, D. Bellet, Discontinuous penetration of liquid Ga into grain boundaries of Al polycrystals, Acta Mater. 52 (2004) 321.
[22] H.-S. Nam, D.J. Srolovitz, Molecular dynamics simulation of Ga penetration along $$\Sigma${}5$ symmetric tilt grain boundaries in an Al bicrystal, Phys. Rev. B 76 (2007) 184114.
[23] H.-S. Nam, D.J. Srolovitz, Effect of material properties on liquid metal embrittlement in the Al–Ga system, Acta Mater. 57 (2009) 1546.